The Characterization and Analysis of A Pseudo Single-grained Copper Impact Weld Interface in Regards to the Effects of Severe Plastic Deformation

Main Author: Taylor Dittrich[1],

Advised by: Glenn Daehn[1], Taeseon Lee[1], and Anupam Vivek[1],

Keywords

Vaporizing Foil Actuator Welding, Explosive Welding, Impact Welding, Characterization

Abstract

Characteristic features of impact welding were explored in regards to the vaporizing foil actuator welding of pseudo single-grained copper sheets. 1/8 hard oxygen free high conductivity copper sheets at various thicknesses were annealed so that abnormal grain growth would occur and simulate a single-grained microstructure. The 0.063" thick sheet was welded to itself using VFAW with an input energy of 10kJ and a standoff distance of 3mm. Optical microscopy was performed on the weld interface at the center of the foil blast, and it showed a clean interface that easily held several characteristic features of impact welding. Electron backscatter diffraction gave a clearer picture of the weld interface, which included deformation twinning, dynamic recrystallization, possible shear banding or nano-twinning, localized melting, and localized grain growth due to heating. Thus, the use of pseudo single-grained materials in impact welding was shown to clearly reveal interface features in impact welding, which will aid in future simulation, experiments, and industry adaptation of impact welding.

[1] Department of Materials Science and Engineering, The Ohio State University, 2041 College Road, Columbus, OH, USA 43210

1. Introduction

1.1 Motivation

The motivation behind this project was to use a pseudo single-grained impact weld system to remove background noise due to initial grain boundaries and gain a clear view of the characteristic microstructural features of impact welding using vaporizing foil actuator welding.

1.2 Vaporizing Foil Actuator Welding

The melting dissimilar metals in conventional welding causes problems because brittle intermetallic compounds are often formed, decreasing the strength of the weld. Impact welding, otherwise known as collision welding, is a solid-state process that allow welds to be performed between highly dissimilar materials with little or no local melting. This process occurs when one sheet of metal collides with another at an appropriate velocity and angle, creating a wave formation at the interface. In many types of impact welding, a target piece of metal is held stationary while a flyer piece of metal is propelled into the target by some type of explosive force. When the two materials collide, a jet is formed that removes both surfaces of any oxides or other contaminations, thus allowing direct contact between the sheets and promoting metallurgical bonding (Vivek, Hansen, Liu, & Daehn, 2013).

Vaporizing foil actuator welding (VFAW) is a specific type of explosion impact welding that sends a charge through a thin piece of aluminum, which instantly vaporizes and creates the pressure/plasma needed for impact welding. It is a relatively clean process that is easily producible in a lab environment, making it ideal for experiments regarding the interface microstructure of impact welding. A schematic of the VFAW setup and process can be seen below as Figure 1.

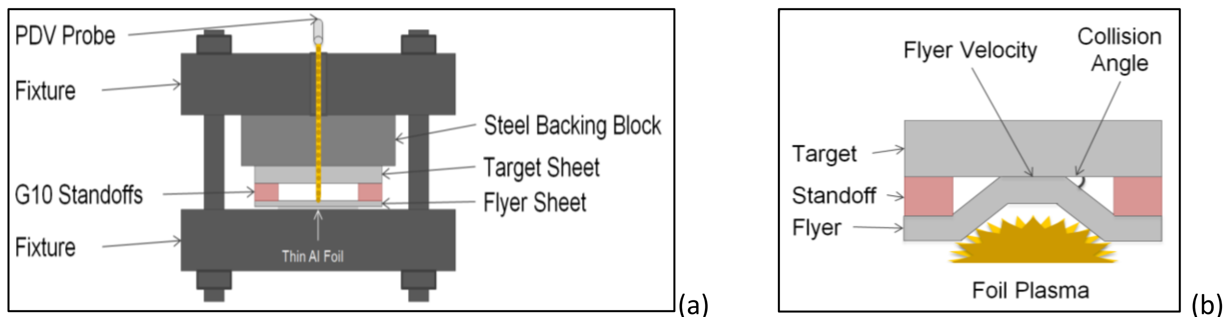

Figure 1: *VFAW (a) setup and (b) process.*

Several simulations that have been performed with the VFAW process indicate areas with the highest effective plastic strain and highest temperature along the weld interface. These regions often correspond to each other, indicating that heat affected zones along the weld interface are most likely regions that experience the most plastic strain. This is demonstrated in Figure 2, showing a simulation for a copper-titanium weld (Nassiri et al., 2017).

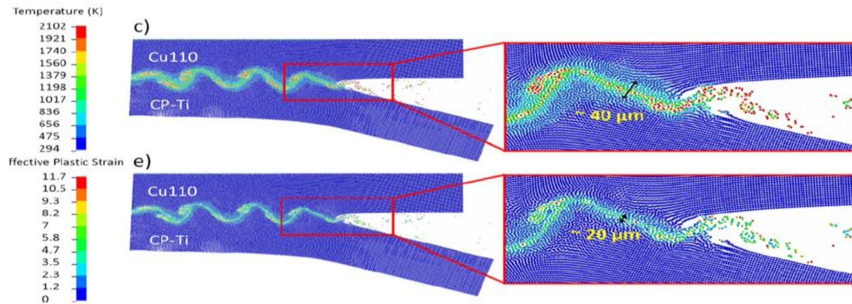

Figure 2: *Predicted field variables for temperature and plastic strain (Nassiri et al., 2017).*

In the VFAW process, the velocity can be measured by utilizing photon Doppler velocimetry (PDV). In PDV, the "interference of original and reflected, Doppler-shifter laser light" is used to track the flyer metal as it accelerates through a standoff distance. This technique is an easy laboratory method for measuring velocity with "high temporal and spatial resolution" by measuring the beat frequency of the interference of the original and reflected light and then converting it to velocity. This acquisition method allows velocity, time, and distance information to be collected and used for collision angle analysis (Vivek, Hansen, & Daehn, 2014).

1.3 Abnormal Grain Growth of OFHC Copper

In order to simulate a pseudo single-grained material for the VFA welding, oxygen free high conductivity copper needed to be annealed to cause abnormal grain growth. Abnormal grain growth occurs when a few grains in an unstable microstructure undergo preferential growth and consume the smaller grains around them. This type of growth doesn't occur in an "ideal grain assembly," but with certain amounts of strain energy, defects, and high annealing temperatures over long periods of time, it may occur (Humphreys & Hatherly, 1995). A coarsening of the grains at high annealing temperatures causes local destabilization of the grain boundaries, which leads to a large grain size distribution where abnormal grain growth can occur. An increase in types of texture will also increase the likelihood of abnormal grain growth as one of the textures will have boundaries with a higher energy and mobility that will migrate preferentially and start abnormal grain growth. Additionally, prior deformation can increase the likelihood of abnormal grain growth as it can promote "anomalous grain growth" by "strain induced boundary migration" (Humphreys & Hatherly, 1995).

The intentional initiation of abnormal grain growth is not a well-studied subject, but the accidental initiation and ways to prevent abnormal grain growth are more prevalent. In annealing experiments by Fullman and Fisher, OFHC copper was annealed for 18 hours at 1040°C in hydrogen to get an average grain size of 0.9mm and annealed for 1 hour at 800°C in hydrogen to get an average grain size of 0.21mm (Fullman & Fisher, 1951). In another set of experiments, pure copper was processed using shear and then annealed at various temperatures to determine the onset of rapid grain growth, which always occurred at relatively high temperatures (Haouaoui, Hartwig, & Payzant, 2005). Other experiments on OFHC copper showed that annealing machined copper at 600°C for over four hours resulted in average grain sizes of 62um (Tanner & McDowell, 1999). All of these experiments confirm

that the onset of abnormal grain growth occurs at temperatures close the melting temperature (1083°C) held for a long period of time with copper that holds a specific amount of strain energy.

1.4 Dynamic Recrystallization and Shear Banding

Dynamic recrystallization is a recrystallization method that occurs at high strain rates, large flow stresses, and high plastic strains in which fine recrystallized grains are observed (often within shear bands). It is associated with an adiabatic rise in temperature and a localization of shear to cause low dislocation density equiaxed grains (Andrade, Meyers, Vecchio, & Chokshi, 1994). Continuous dynamic recrystallization occurs due to severe plastic deformation from high strain rates and high plastic strains, which changes the dislocation structure in those areas of localized shear. The driving force for dynamic recrystallization is the dislocation energy generated from that severe plastic deformation, and the formation of smaller, low dislocation grains becomes more favorable to reduce free energy. The plastic deformation increases the dislocation density until an unstable dislocation structure is formed, which then causes low angle sub-grains to form (Bacca, Hayhurst, & McMeeking, 2015). As further deformation progresses, the sub-grains will break up into micrograins. Minor rotations of the grain boundaries will then cause these micrograins to become equiaxed through a rotational recrystallization mechanism. This dynamic rotational recrystallization process can occur both after deformation and during severe plastic deformation (Meyers, Nesterenko, LaSalvia, Xu, & Xue, 2000).

The phenomena of dynamic recrystallization is documented to occur within many types of shear bands but notably in the shear bands of copper, where small equiaxed grains exist inside the shear bands (Meyers et al., 2000). Adiabatic shear bands are comprised of “concentration[s] of deformation in narrow bands” and are formed through the competition between dislocation multiplication (strain hardening), thermal softening from plastic work, and dynamic recovery/dyamic recrystallization (Boakye-Yiadom & Bassim, 2018). High shear deformation will localize within the shear bands, causing work hardening with an increase in dislocation density; but it will be offset by dynamic recrystallization that decreases the dislocation density within small equiaxed grains (Tang et al., 2012). A temperature rise in an area of deformation can cause instability and the localization of shear, but the role of temperature in shear band formation is not conclusive. It has been found that plastic flow instability is one of the necessary conditions for adiabatic shear bands to form at high strain rates and plastic deformations. Dislocations will form cell structures and substructures at high strain rates and then may undergo dislocation-nucleation controlled softening and micro-twining. Shear bands can be formed without the occurrence of dynamic recrystallization, indicating that thermally activated processes and dynamic recrystallization may not be triggers for shear banding. However, dynamic recrystallization will still often occur alongside shear banding (Boakye-Yiadom & Bassim, 2018).

1.5 Deformation-induced Twinning and Nano-twinning

Deformation twinning in FCC materials relies on high localized stresses to cause the movement of partial Shockley dislocations from grain boundaries to shear planes of atoms across a specific deformation axis and create a mirror image with the parent grain. The occurrence of twinning relies heavily on stacking fault energy, temperature, and strain rate. Because of the high stacking fault energy of copper, the

nucleation and growth of deformation twins occurs either at extremely low temperatures or at high strain rates because thermally-activated dislocation processes (such as dynamic recrystallization and grain boundary migration) are subdued (Boakye-Yiadom & Bassim, 2018). Deformation twinning in FCC metals will often occur on the {111} planes (Humphreys & Hatherly, 1995). It will also cause a regular misorientation angle of 60° across the deformation twin boundaries with the parent grain (Tang et al., 2012).

The nucleation of nano-twinning is similar to that of larger deformation twinning in that it relies of the propagation of partial dislocations on the {111} planes. However, a nano-twinned structure results from a change in the local stacking sequence from FCC to HCP for a layer of atoms. Similar to larger deformation twinning, nano-twining will only occur in high stacking fault energy metals at high strain rates or low temperatures. It has been hypothesized that nano-twinning can occur at the same time as slip/shear of perfect dislocations (Sun, He, & Lu, 2018).

2. Experimental Methods

2.1 Annealing of OFHC Copper

Four different combinations of tempers and thicknesses of oxygen free high conductivity copper were used in this experiment: 1/8 hard 0.032" thick, 1/8 hard 0.063" thick, 1/8 hard 0.093" thick, and full hard 0.063" thick. Based on previous literature review, an initial annealing temperature of 850°C, annealing time of 7 hours, and furnace cool overnight were chosen for the initial annealing trial of each combination of temper and thickness. The annealing was performed in a standard furnace with the bars sectioned into 1" x 1.5" samples. The samples were stacked on top of each other, covered with charcoal, and wrapped with a thin layer of copper to getter oxygen. Following microstructural analysis of those samples, it was decided to attempt annealing at a temperature closer to the melting point of OFHC copper (1083°C). A second annealing trial was performed at 950°C for 9 hours with the same conditions as the previous annealing trial. Microstructural analysis proved that this annealing time and temperature was sufficient for abnormal grain growth to simulate a single-grained structure. The grain size analysis of both annealing trials can be found in Appendix A.

However, due to the long annealing time and high annealing temperature, a thick oxide layer formed on the surface of the samples. It was decided that a vacuum furnace would be used for annealing the actual weld samples. The OFHC copper was sectioned into 2" by 3" coupons so that there were multiple coupons for all the 1/8 temper copper thicknesses. These coupons were arranged vertically in a ceramic cup, placed into a vacuum furnace, and brought to vacuum under 1 torr. An automatic annealing cycle was run with the following parameters: 30 minute ramp up to 950°C, hold for 8.5 hours, 30 minute ramp down to room temperature, and vacuum cool overnight.

Additional OFHC copper coupons were annealed for PDV analysis with the same parameters as the other vacuum furnace samples. However, due to concerns about the protection the heating elements in the vacuum furnace, the furnace was backfilled with argon. No other changes were made to the annealing

procedure. In total, four 2” by 3” coupons were annealed using argon gas, half being the 1/8 temper 0.032” and the other half being the 1/8 temper 0.063”.

2.2 VFAW and PDV

The VFAW parameters used for welding the annealed copper 0.063” flyer to another annealed copper 0.063” target are as follows: 0.003” thick patch foil (shown below in Figure 3), 3mm standoff distance made by two layers of 1.5mm thick G10, 10kJ of input energy. This weld was performed once for microscopic analysis and a second time with only the flyer for PDV analysis. Additionally, a weld with between an annealed copper 0.032” flyer to an annealed copper 0.093 target was performed with the same weld parameters as the 0.063” to 0.063” weld. PDV was not performed on this 0.032” to 0.093” weld.

PDV analysis was performed using only the argon-annealed copper 0.063” flyer because the target was unnecessary to measure velocity or estimate collision angles. Two PDV probes were placed perpendicular to the flyer spaced 3.8mm apart from each other, and a backing block with an off-center hole that spanned half the width of the copper target was used to allow the probes to reach the flyer surface. During the PDV analysis, the VFAW process was performed with the same parameters as the annealed copper 0.063” to 0.063” weld. The collision angle 3.8mm away from the center of the weld was determined using the velocity-time data from PDV and a basic geometric analysis.

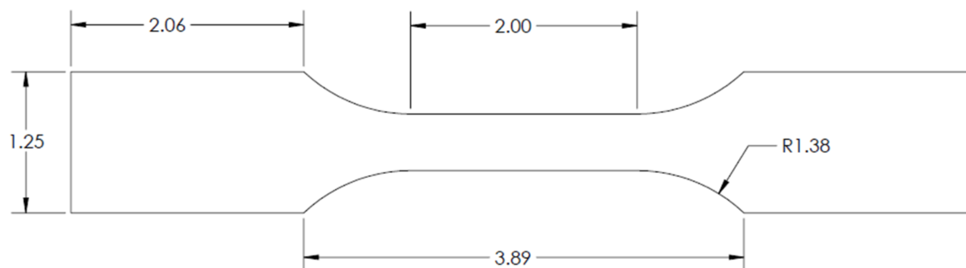

Figure 3: *0.003” thick aluminum patch foil.*

2.3 Optical Microscopy

Once the two welds were created using the VFAW process, they were sectioned to reveal the weld interface along the center of the aluminum foil. Standard metallographic procedures were followed to mount the samples in conductive bake light and grind/polish away previous layers of deformation. It should be noted that only ethanol, not water, was used in the grinding and polishing process. Final polishing steps were completed with 0.05 colloidal silica for 10 minutes so that the sample etched slightly. Following final polishing, the annealed copper sheets were etched with a solution of equal parts 3% hydrogen peroxide, distilled water, and ammonium hydroxide for roughly 30 seconds. A new etchant was mixed every fifteen minutes as potency of the etchant was lost over time.

2.4 Electron Backscatter Diffraction

After undergoing optical microscopy, the weld samples were re-polished carefully using the same procedures as the initial polishing. The slight etch from the colloidal silica aided in optimizing data from the EBSD scans. The samples were placed into the new FEI Apreo FEG scanning electron microscopes located at the Ohio State Center for Electron Microscopy and Analysis (CEMAS). These SEMs were equipped with EDAX high-speed Hikari electron backscatter diffraction (EBSD) cameras, and TEAM software was used for data collection in this experiment. EBSD was performed at various magnifications along the weld interfaces with an accelerating voltage of 10kV, a beam current of 13nA, and 5x5 binning.

3. Results

3.1 Macro Results

The macroscopic annealing results from the vacuum annealing at 950°C for 8.5 hours for the 1/8 hard 0.063" thick copper can be seen in Figure 4. Optically, it can be seen that the 0.063" thickness had an annealed structure of abnormally large grains surrounded by smaller grains. The abnormally large grains could reach sizes as large as 1.5 cm. Combined with the cross-sectional analysis of the initial annealing trial at 950°C, the 0.063" to 0.063" weld was chosen as the focus for advanced characterization with EBSD. Although not the main focus of this paper, macro, micro, and EBSD results from the 0.032" to 0.093" weld can also be seen in Appendix B.

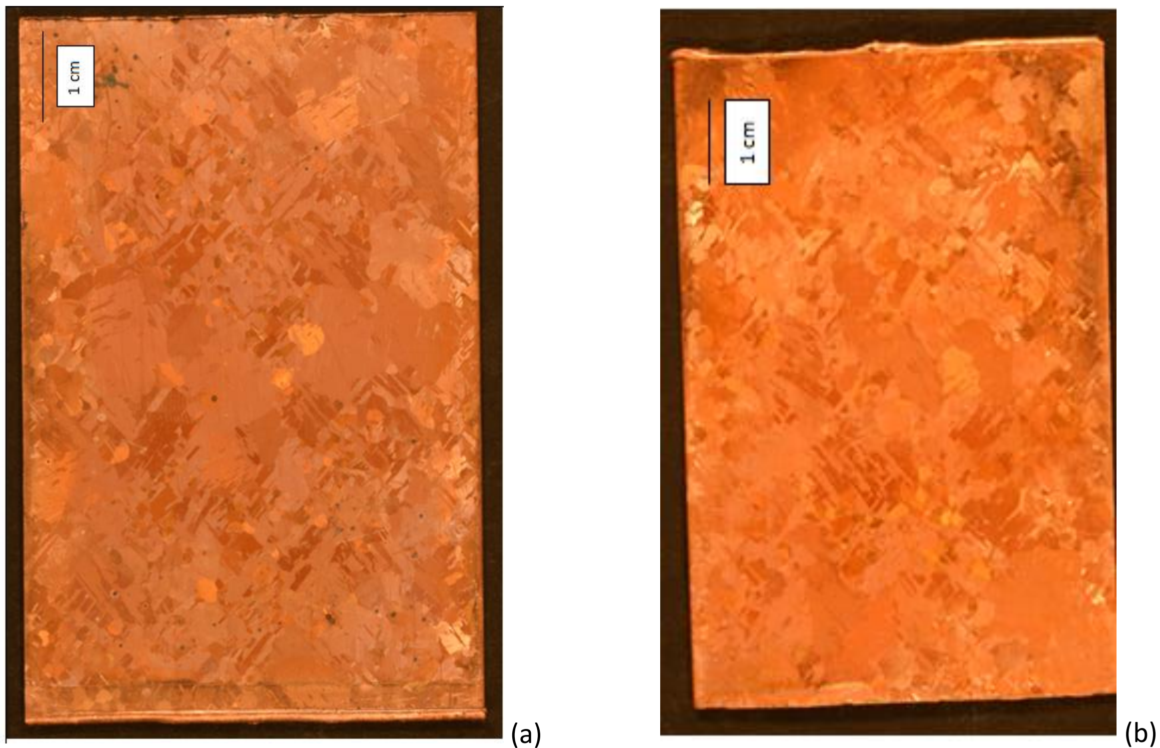

Figure 4: *Annealed copper sheets of the (a) flyer and (b) target*

Macro-images of the 0.063” to 0.063” weld can be seen in Figure 5. These images demonstrate that the two materials welded easily, and the impact welding process caused a lot of deformation along the welded regions. Clear deformation twinning, grain refinement, and various other methods of strain accommodation can be seen at a macro level. Tactilely, the ridges formed from the welding process can be clearly felt and describe the high amount of strain accommodation that occurs in these impact welds.

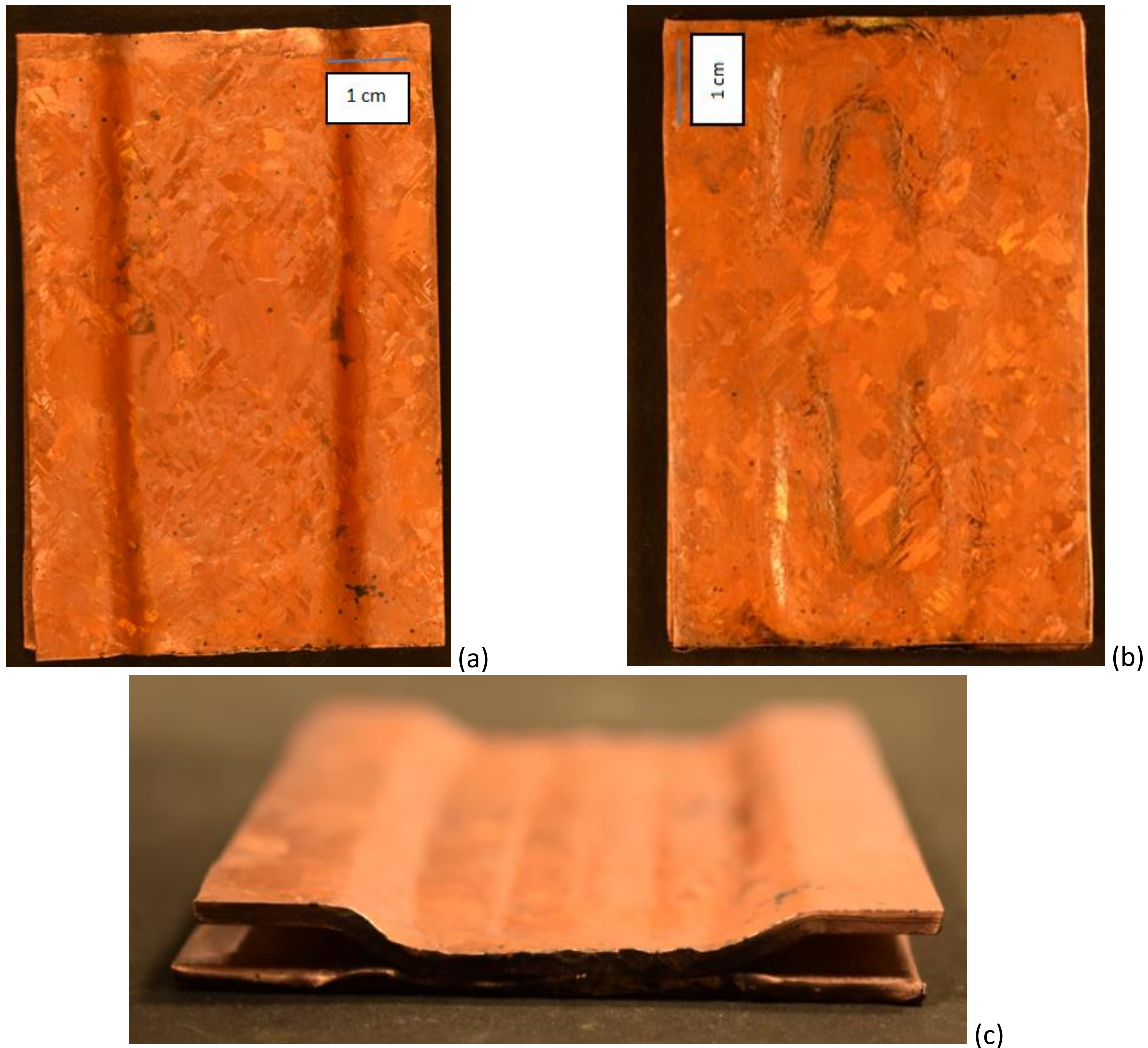

Figure 5: *Welded 0.063” to 0.063”, showing the (a) back of the flyer, (b) back of the target, and (c) the whole weld.*

3.2 PDV and Collision Angle Results

The velocity at various points along the weld interface was determined using multi-channel PDV and used to estimate the collision angle of the impact weld. This data can be seen below in Table 1, and the velocity and collision angle remain well in the region of weldability, especially for soft, pure copper. If more information on the impact velocity and collision angle is needed, figures on the velocity versus distance, frequency versus time, and the actual calculation of the collision angle is in Appendix C.

Table 1: *PDV and collision angle results for 0.063" flyer with 0.003" foil and 10kJ of energy.*

PDV Results		
	C1 (center)	C2 (offset)
Velocity (m/s)	260	220
Collision Angle (rad)	-	0.18
Collision Angle (deg)	-	10.19

3.3 Optical Microscopy

Optical micrographs were taken from the cut, mounted, polished, and etched sample of the 0.063" to 0.063" annealed copper weld, and these images can be seen in Figures 6 and 7. These micrographs show an interface that is relatively free of previous grain boundaries and reveals various features of impact welding along the weld interface. These features potentially include deformation twinning, the shearing of annealing twins, dynamic recrystallization, shear banding or nano-twinning, localized melting, and localized heating. However, these features could not be confirmed with only optical microscopy because it is unable to resolve very fine grains and features. More advanced characterization with EBSD was needed to give information about the extremely fine grains and grain orientation.

Figure 6: *Optical micrograph at 100x of 0.063" to 0.063" annealed copper weld.*

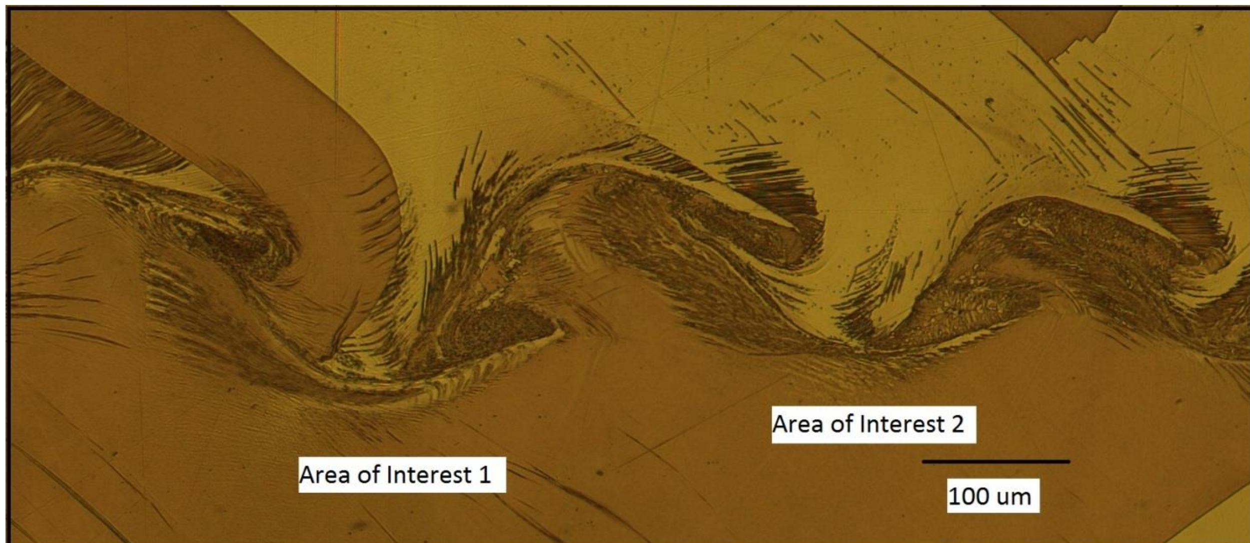

Figure 7: *Optical micrograph at 200x of regions of interest in 0.063" to 0.063" weld.*

3.4 Electron Backscatter Diffraction

EBSD analysis was focused on the two different regions of interest shown in the above optical micrograph: area one with a large amount of deformation twinning and dynamic recrystallization, and area two with a large amount of shear banding/nano-twinning and regions of local melting/heating. An ipf of area one, shown as Figure 8, reveals a sheared annealing twin and deformation-induced twining, along with several other microstructure features that could not be resolved at the low magnification. Attempts to quantitatively confirm the twinning were made using the OIM software, but the software was unable to recognize any twins in Figure 8 with the following FCC deformation twinning parameter: 60° misorientation about the [111] axis. Because a misorientation of 60° was found when the misorientation was measured from point to point across the presumed twins, it seemed that additional shearing occurred to knock the deformation twins off the [111] axis. Most of the presumed deformation twins exhibited this behavior; but there were also areas that showed a uniform orientation change but did not exhibit a misorientation close to 60°, indicating that they were not areas of deformation twinning. Deformation twinning in this experiment was defined as regions where the misorientation measured from point to point equaled around 60°. A twinned region, a non-twinned region, and their misorientation profiles can be seen in Figures 8 and 9.

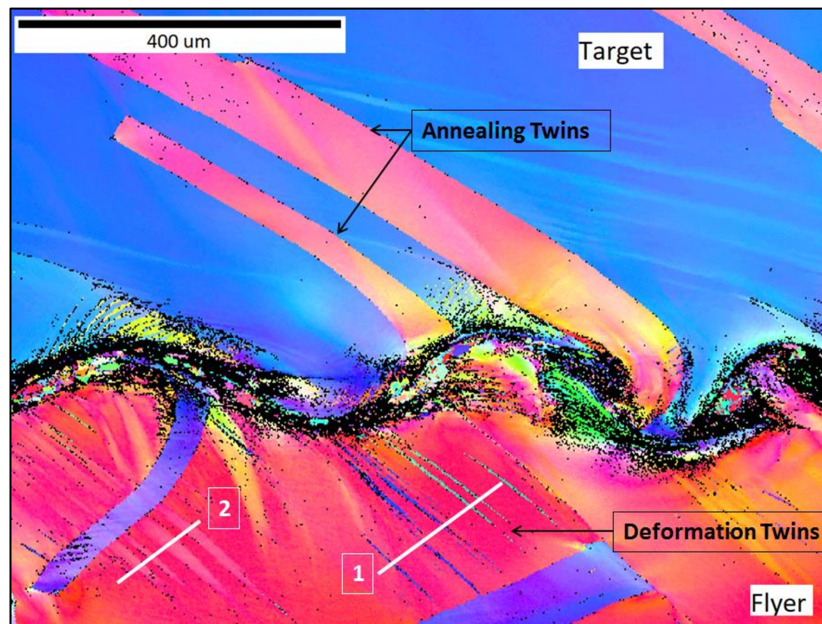

Figure 8: *Low mag. ipf of area one, partitioned to remove low CI grains and labeled with areas of measured misorientation.*

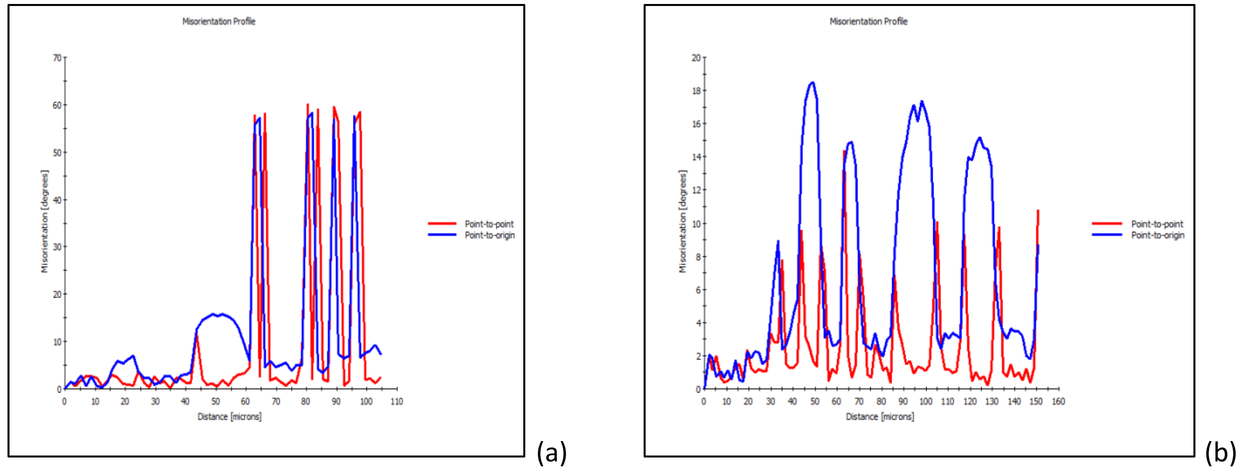

Figure 9: *Misorientation profiles along (a) line [1] and (b) line [2] in area of interest one.*

Higher magnification EBSD scans also revealed regions with deformation twinning and possibly some shear banding or nano-twinning. An ipf and the measured misorientation profiles across potential twinned regions can seen be in Figures 10 and 11, but additional ipfs may be seen in Appendix D, along with the failed results from the software fitting of deformation twins. A higher magnification ipf of area one (Figure 12) also shows a region of distinct dynamic recrystallization, identified through its intense grain refinement due to severe plastic deformation.

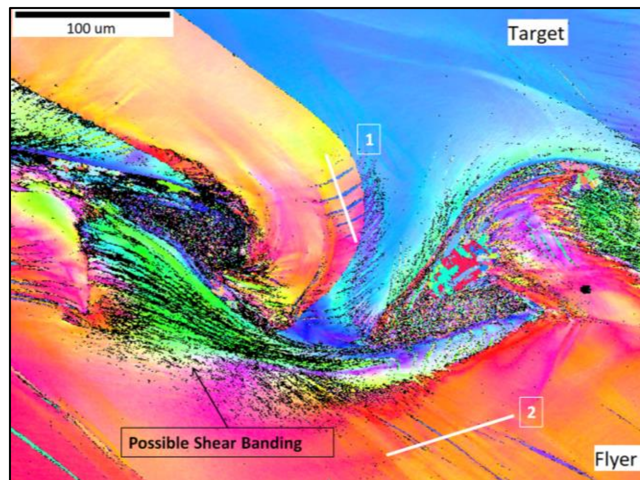

Figure 10: *Medium mag. ipf of area one, showing deformation twinning and possible shear banding.*

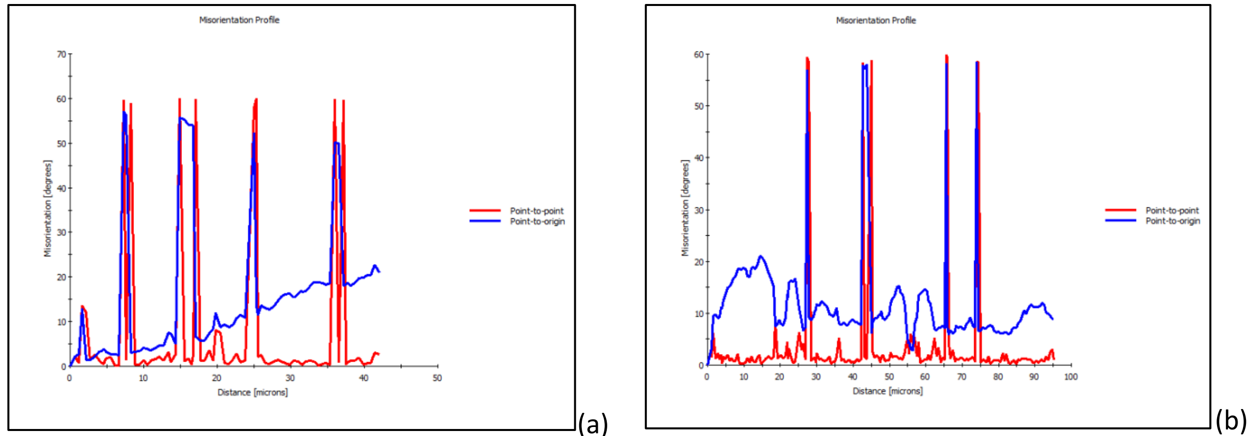

Figure 11: *Misorientation profiles along (a) line [1] and (b) line [2] in area of interest one.*

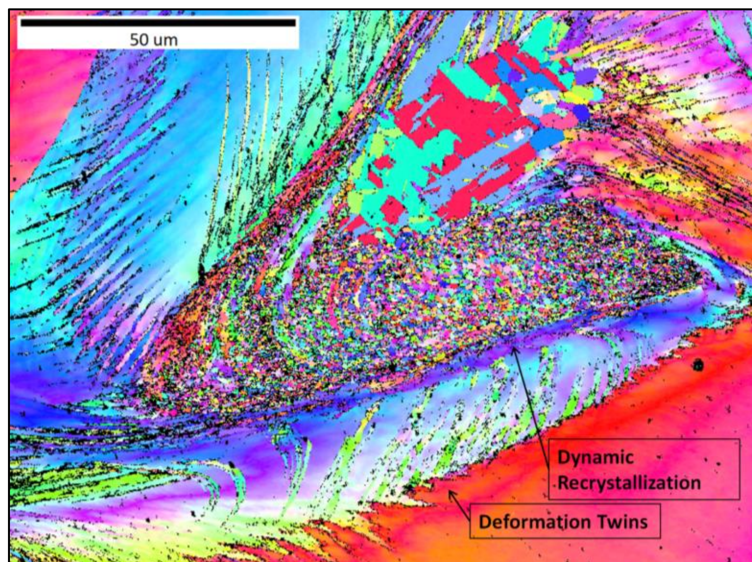

Figure 12: *High mag. ipf of area one, showing deformation twinning and dynamic recrystallization.*

EBSD analysis of area two (Figure 13) also reveals regions that seemed to consist of a mixture of deformation twinning and shear banding along the weld interface. As seen in Figures 14, narrow deformation twinning was confirmed with a misorientation measurement. However, intense grain refinement along narrow banded regions was also observed, indicating the presence of shear banding/nano-twinning.

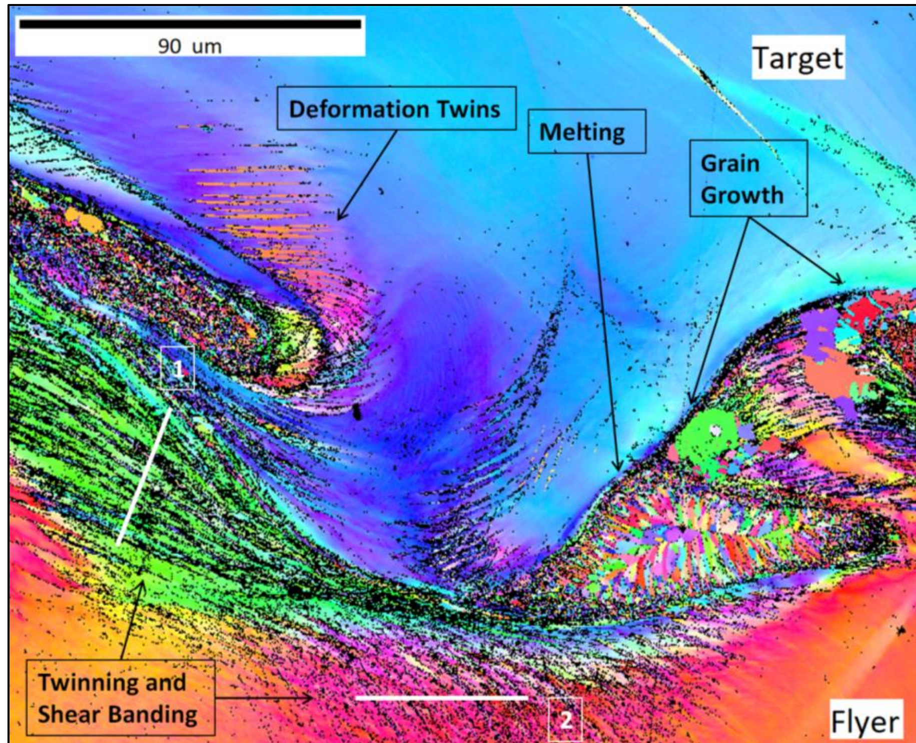

Figure 13: *Medium mag. ipf of area two, showing deformation twinning, shear banding, heating, and melting.*

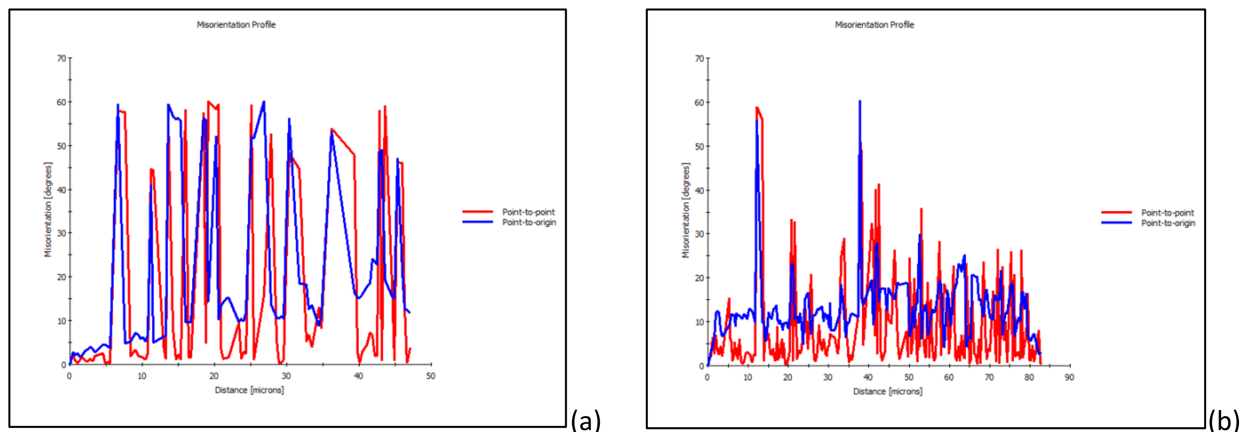

Figure 14: Misorientation profiles along (a) line [1] and (b) line [2] in area of interest two.

A higher magnified ipf of area two (Figure 15) showed a region local melting, which was confirmed by the clear solidification line and the solidification direction of the resultant grains. This local melted region occurred in waves located closer to the center of the weld, which experience more pressure from the initial foil vaporization. The melted region also formed in a region under the wave crest that has often been predicted to experience the highest amount of strain (Nassiri et al., 2017). Additionally, Figure 15 shows areas where grain growth occurred from high temperatures that did not actually melt the metal. According to simulation results for dissimilar impact welds, these regions also correspond to areas of high strain, (Nassiri et al., 2017).

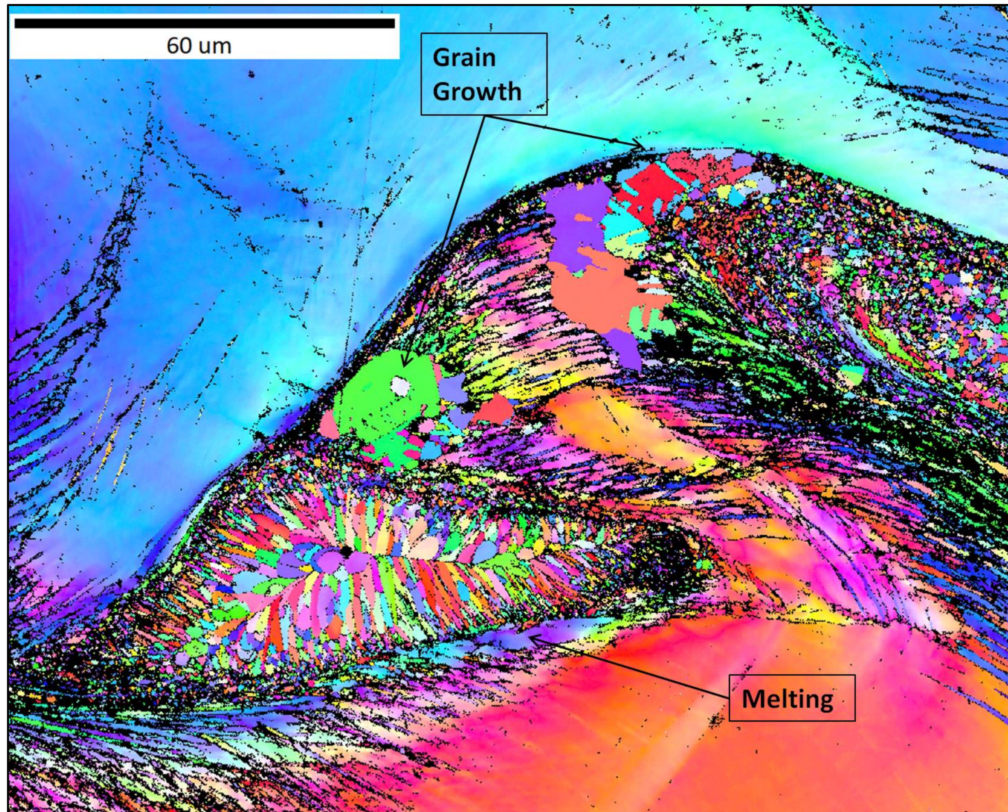

Figure 15: *High mag. ipf of area two, showing local melting and heating-induced grain growth.*

4. Discussion

4.1 Deformation-induced Twinning and Shear banding

In many of the inverse pole figures, deformation twinning can be easily seen as a uniform change of orientation across a relatively straight or elliptical line. Optically, these regions are clearly identified as deformation twinning that occurs due to the high amount of strain and high strain rate involved in the VFAW process. As deformation twinning often occurs along the [111] axis and results in a 60° misorientation in FCC materials, attempts were made to confirm these visual twins using software analysis. However, even when the misorientation tolerance was increased, the OIM software was unable to conclude that the visual twins were deformation twins based on the regular deformation twinning parameters for FCC copper. This lead to the theory that the twinning was not present along the [111] axis because the twins formed and then further sheared off the [111] axis onto some other plane due to the large amount of strain involved in the welding process. Based on this theory, if the misorientation between the twins and their parent grains was found to be close to the regular angle of 60°, those visual twins must actually be deformation twins that sheared off their regular [111] axis.

In almost all the areas measured, this did seem to be the case with the notable exceptions of line 1 in Figure 8 and line 2 in Figure 13. The region measured in line 2 of Figure 13 included many refined grains

that could not be resolved with EBSD that occurred along distinct band regions, similar to the band regions found along the misorientation measurement of line 1 in the same figure. However, in the case of line 2, most of these lines could not be confirmed to be twins, indicating that some other process must be in place. Perhaps these fine grains are the result of very fine nano-twinning or perhaps they are the result of dynamic recrystallization occurring within shear bands. The presence of shear banding is difficult to differentiate from other deformation features in copper, and nano-twinning is difficult to resolve in regular EBSD. Thus, while it is clear that these areas of intense grain refinement along band regions are not due to conventional deformation twinning, it cannot be confirmed as to whether they are the result of nano-twinning or shear banding. As fcc copper may experience both of these deformation structures, the best theory at this time is that these areas are the result of a combination of both deformation nano-twinning and dynamic recrystallization in shear bands. Future analysis with TKD may be able to better illuminate these highly refined narrow regions.

4.2 Dynamic Recrystallization

Along with deformation twinning and possible shear banding/nano-twinning, the weld interface clearly reveals large areas that experienced dynamic recrystallization, shown well in Figure 12. The wave area in which the dynamic recrystallization occurred was at a higher collision angle further away from the center of the weld, and the grain refinement can be seen underneath the wave crest in areas of high plastic strain. Dynamic recrystallization was not observed at all points under the waves in the weld interface but occurred more readily further away from the center of the weld, as dynamic recrystallization is induced by plastic deformation with short cooling times. It seems that areas with a larger collision angle experienced more mixing and rotation under the crest of the waves and likely cooled more quickly, thus allowing subgrain formation and rotational recrystallization to occur in a large region rather than along a narrow shear band (as is often seen in copper subjected to high strain rates).

4.3 Localized Heating and Melting

As areas that are closer to the center of the weld experience more pressure, smaller/no collision angles, less mixing, and stay molten for a longer period of time, they seem less likely to experience dynamic recrystallization and more likely to experience melting or grain growth. These effects can be seen in Figure 15, where localized heating caused areas of pure melting/solidification and heat-induced grain growth. The melted and solidified region in Figure 15 greatly resembles that of more conventional welding (such as resistance spot welding) with a clear solidification line and grain growth out from that solidification line forming a dendritic structure. Additionally, large grain growth occurred in grains that held stored strain energy and experienced increased temperature below the melting point. Instead of undergoing processes like dynamic recrystallization and twinning to relieve strain energy, the grain consumed surrounding grains and grew through diffusion-mediated grain boundary growth.

5. Conclusions

Pseudo single-grained sheets of copper were used in conjunction with the VFAW process to create a clear impact weld interface that revealed several characteristic features of impact welding. Several different deformation-induced strengthening features were discussed, including deformation twinning and dynamic recrystallization, while the presence of nano-twinning and shear banding was hypothesized. Along with strengthening features, local heat affected zones were identified as regions of melting/solidification and grain growth. These undesirable weld features were seen in areas along the weld interface that often corresponded to the highest amount of plastic strain and thus the highest temperature rise. To gain a better understanding of the mixing and position of the interface, pseudo single-grained samples of dissimilar metals should be welded with VFAW and then analyzed in a similar manner to that done in this study. It has been shown that the use of pseudo single-grained metals allows for an easy evaluation of the high strain rate, severe deformation-induced structures found in impact welding.

6. Acknowledgements

Many thanks to the members of the Impulse Manufacturing Lab, including Glenn Daehn, Anupam Vivek, and Taeseon Lee, for their efforts and funding regarding this project. Additional thanks to members of CEMAS, including Jon Orsborn, for technical assistance. Finally, thanks to the College of Engineering for their aid in funding my research.

7. Appendix

A. Air Furnace Annealing Trials

Table 2: *Grain sizes of initial annealing trials determined by line intercept method.*

Grain Size Analysis Air Furnace Trials								
	Full Hard .063"		1/8 Hard .032"		1/8 Hard .063"		1/8 Hard .093"	
Annealing Temp.	850˚C	950˚C	850˚C	950˚C	850˚C	950˚C	850˚C	950˚C
Annealing Time (hrs)	7.00	9.00	7.00	9.00	7.00	9.00	7.00	9.00
Avg. Grain Size (um)	40.28	216.61	355.60	402.68	359.74	844.04	166.64	798.52
Std. Deviation	0.74	69.76	94.90	199.56	38.05	36.76	8.62	135.44

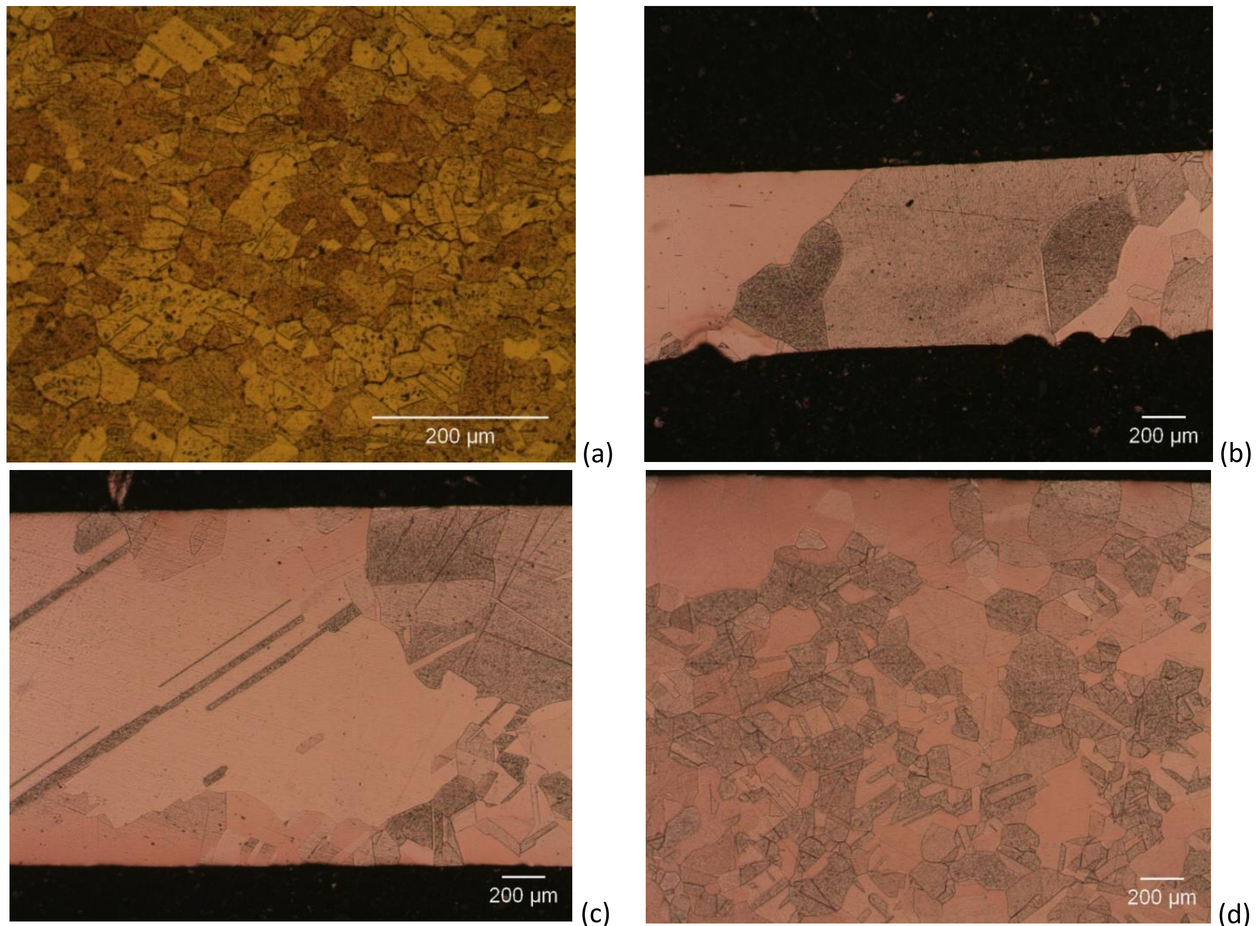

Figure 16: *Annealing 850°C for 7 hrs- (a) full hard 0.063", (b) 1/8 hard 0.032", (c) 1/8 hard 0.063", and (d) 1/8 hard 0.093"*

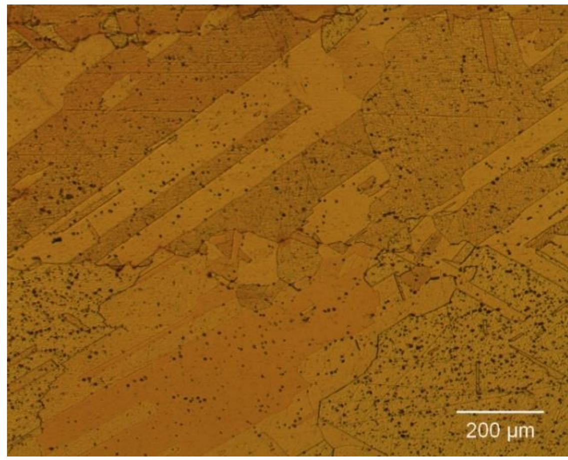

(a)

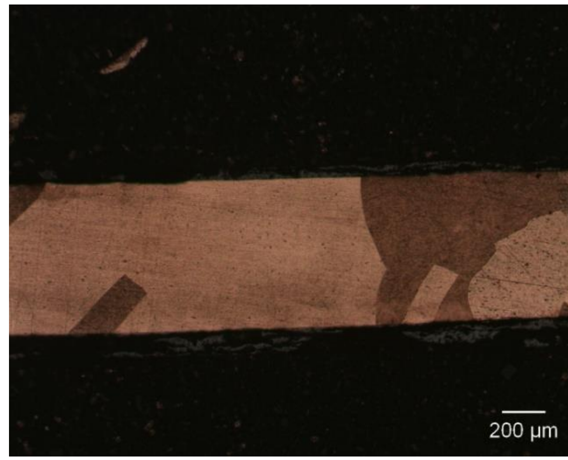

(b)

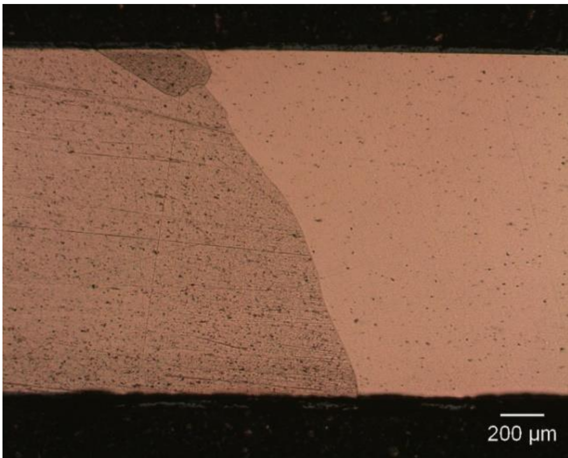

(c)

(d)

***Figure 17**: Annealing 950°C for 9 hrs- (a) full hard 0.063", (b) 1/8 hard 0.032", (c) 1/8 hard 0.063", and (d) 1/8 hard 0.093"*

B. 0.032” to 0.093” Weld

Figure 18: *Macro images of 0.032” to 0.093” annealed copper weld.*

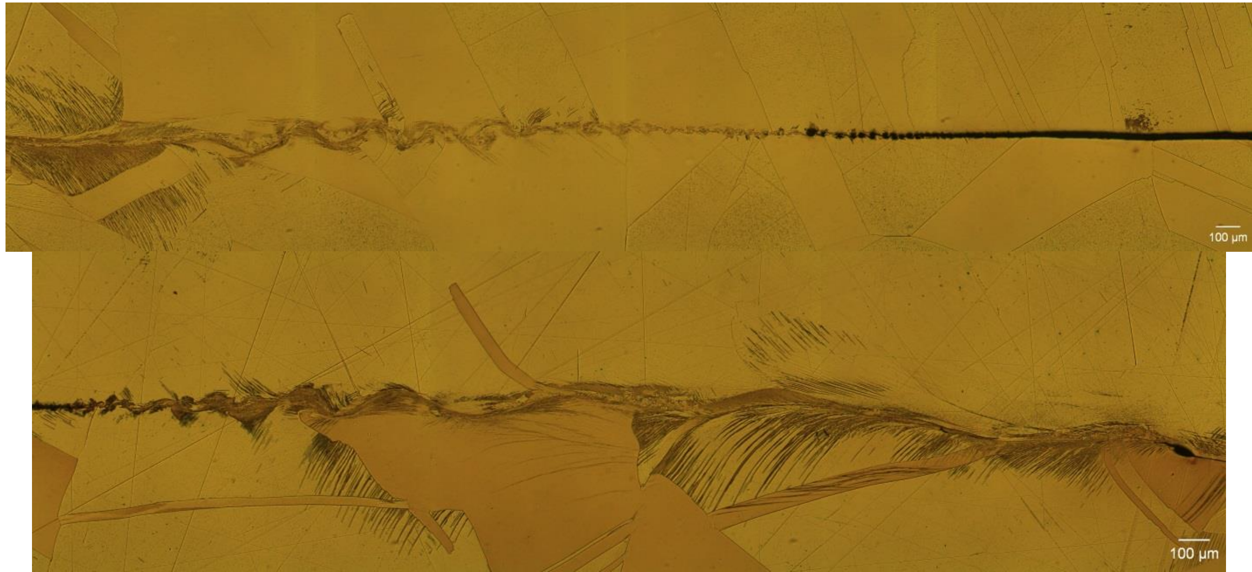

Figure 19: *Optical images of 0.032" to 0.093" annealed copper weld.*

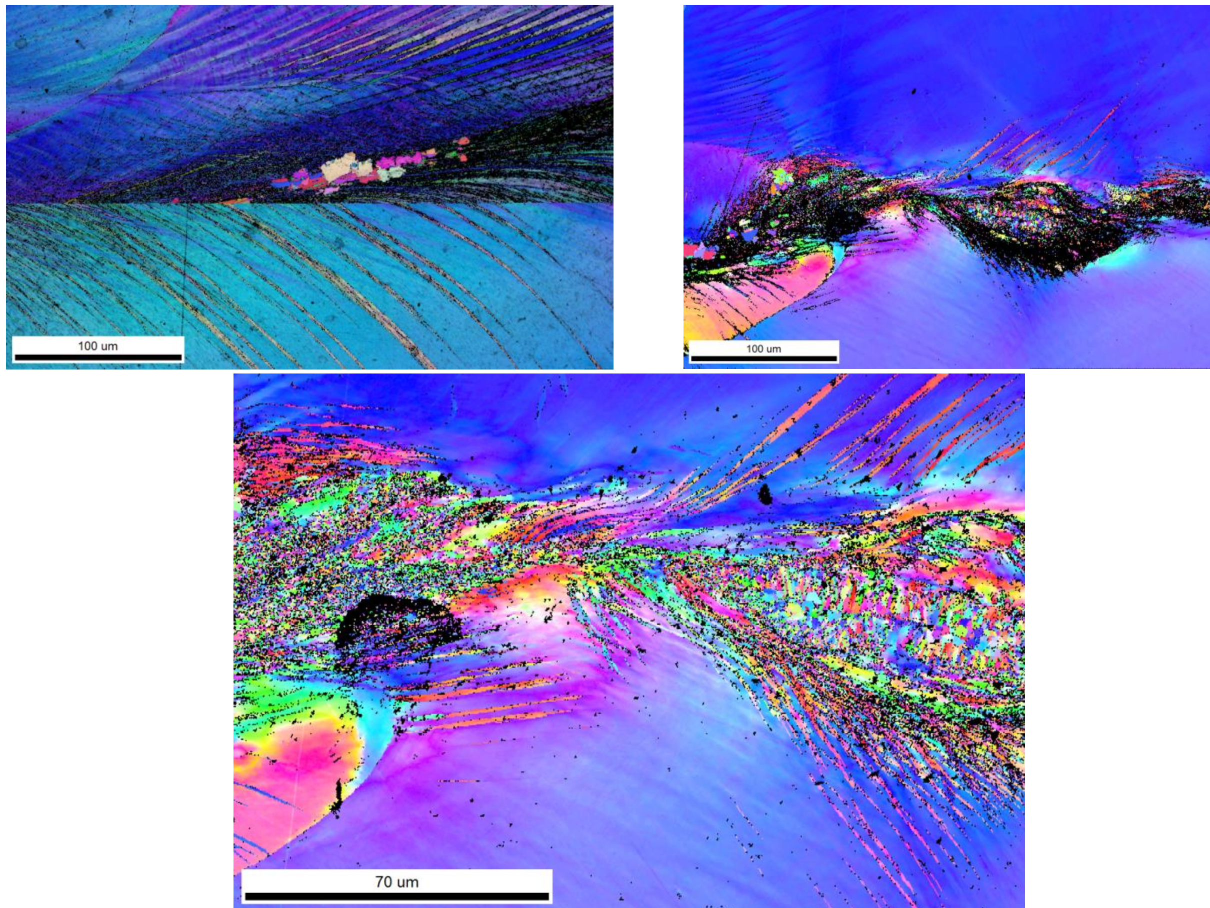

Figure 20: *EBSD ipf images of 0.032" to 0.093" annealed copper weld.*

C. PDV Calculations

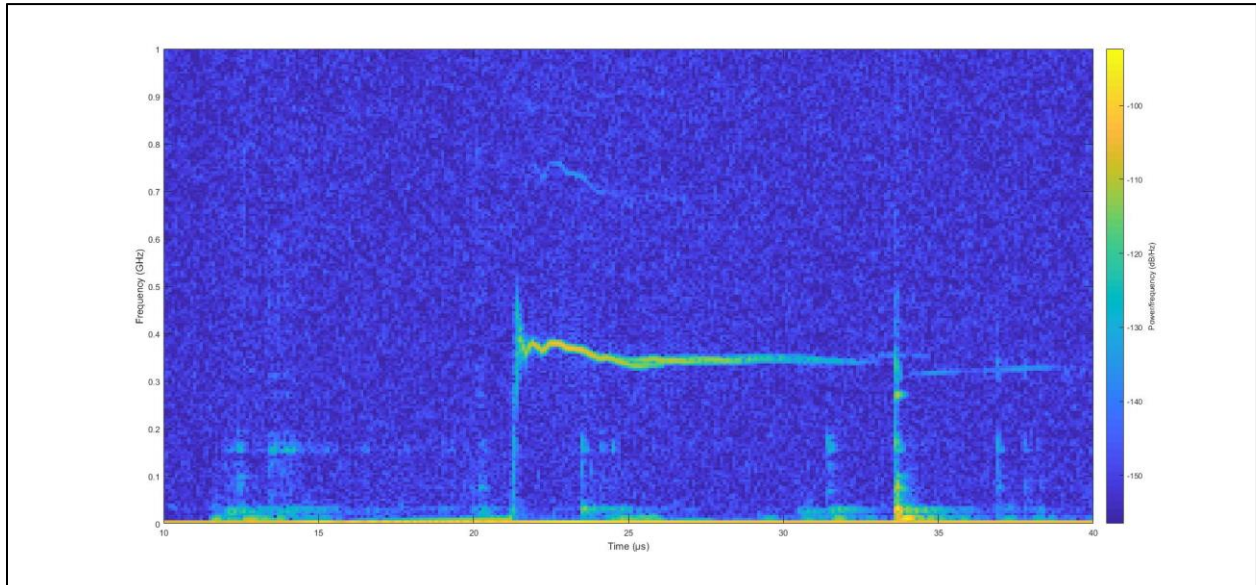

Figure 21: *Frequency vs. time plot for probe C1. Can be used to extract velocity vs. time and velocity vs. distance.*

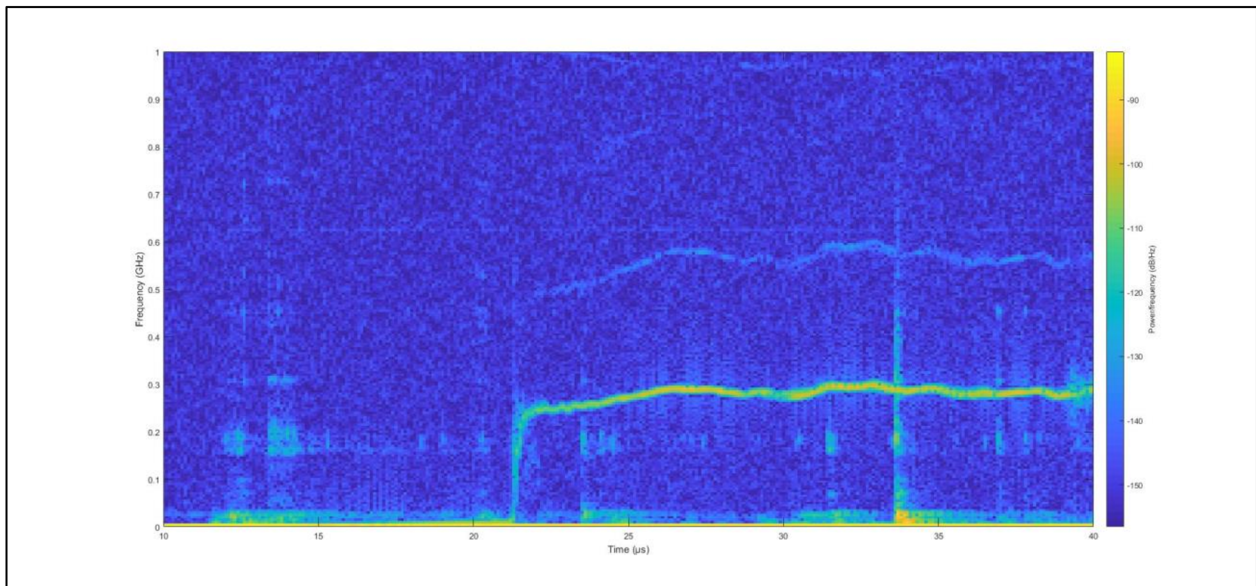

Figure 22: *Frequency vs. time plot for probe C2. Can be used to extract velocity vs. time and velocity vs. distance.*

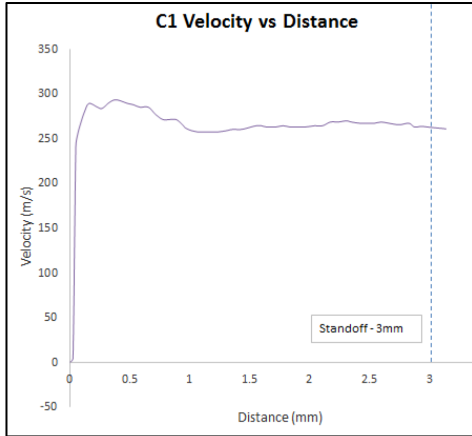

Figure 23: *Velocity vs. distance graph for probe C1.*

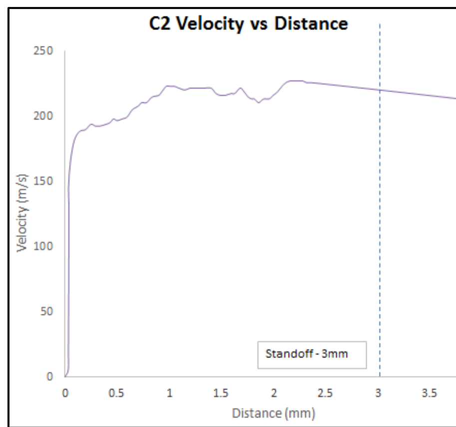

Figure 24: *Velocity vs. distance graph for probe C2.*

Table 3: *Table of distance and time for both probes to reach specified standoff distance of 3 mm.*

	Distance (mm)	
Time (us)	Probe C1	Probe C2
22.30	3	2.315
25.39	3	3

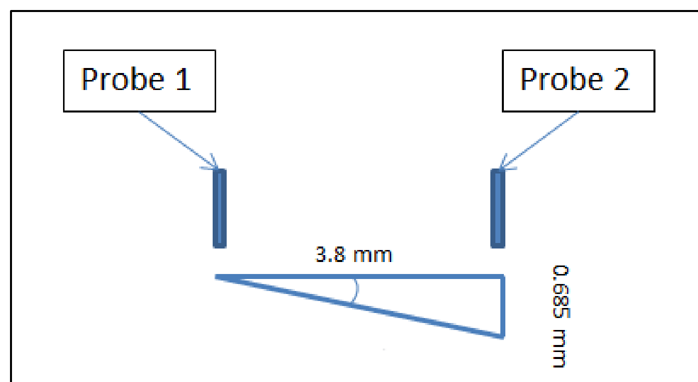

Figure 25: *Triangle of distance between probes to estimate collision angle.*

D. EBSD and Misorientation Profiles of 0.063” to 0.063”

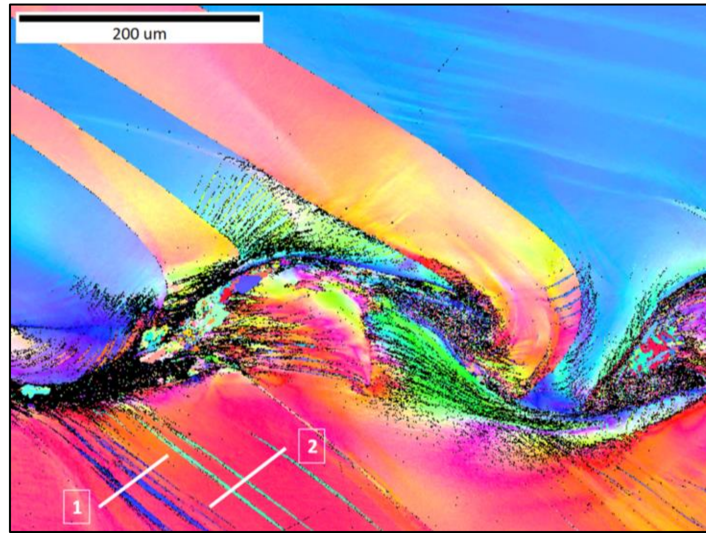

Figure 26: *350x ipf of area one with misorientation measurements.*

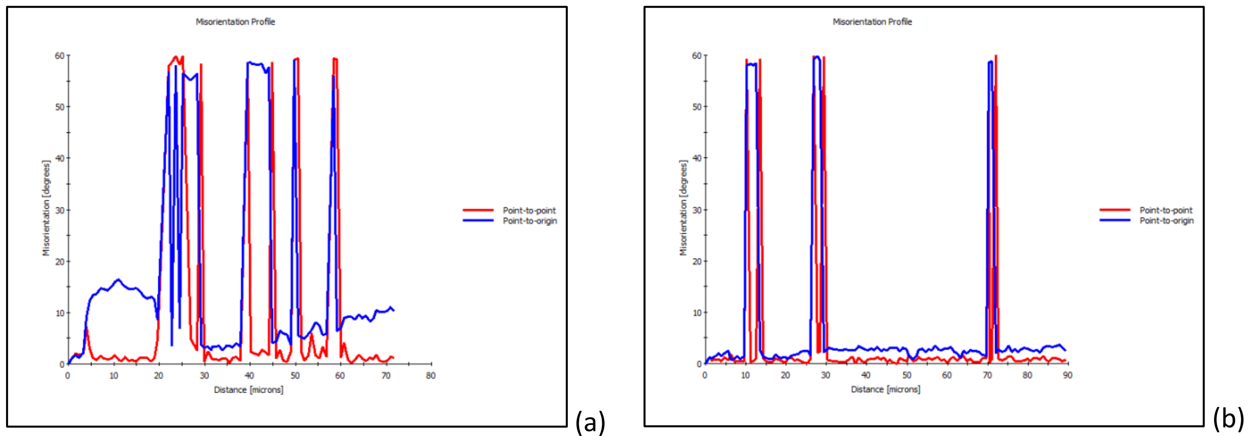

Figure 27: *Misorientation profiles for area one, 350x.*

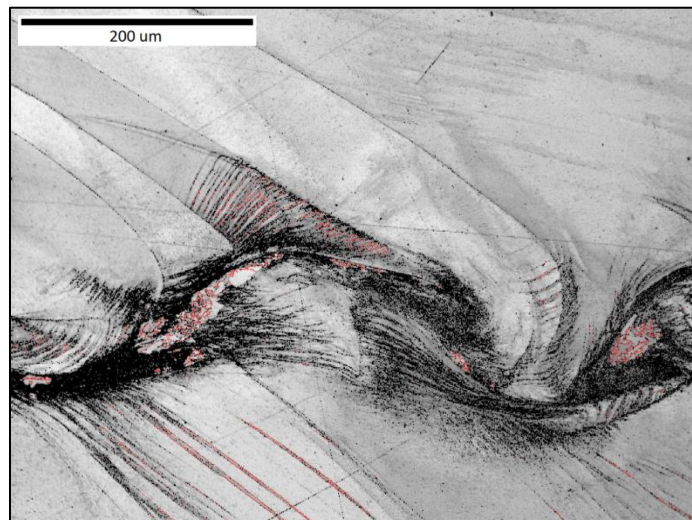

Figure 28: *Software attempt at determining twinning for 350x ipf.*

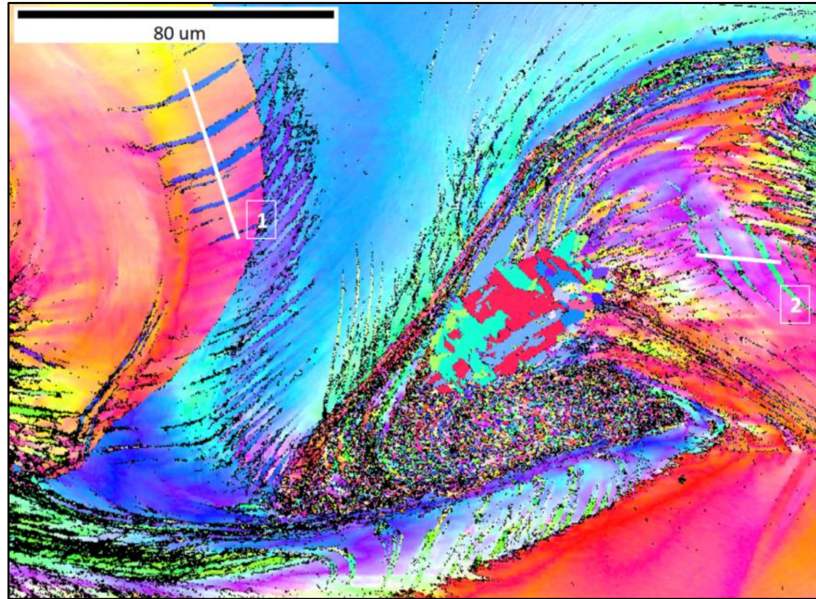

***Figure 29:** 1000x ipf of area one with misorientation measurements.*

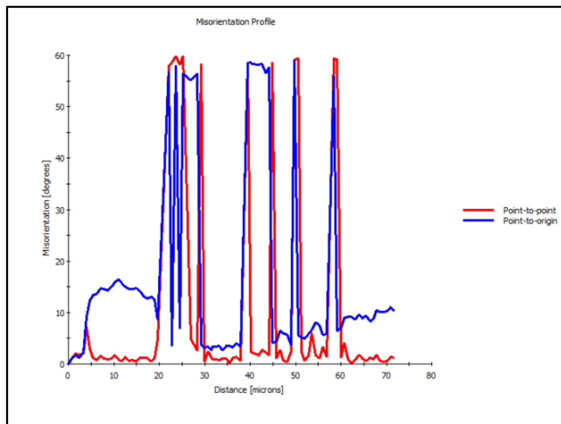

(a)

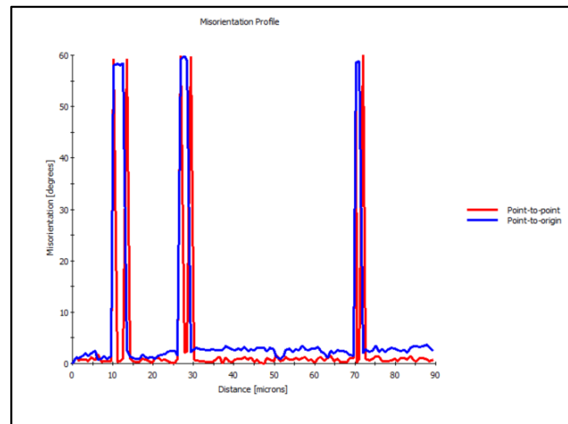

(b)

***Figure 30:** Misorientation profiles for area one, 1000x.*

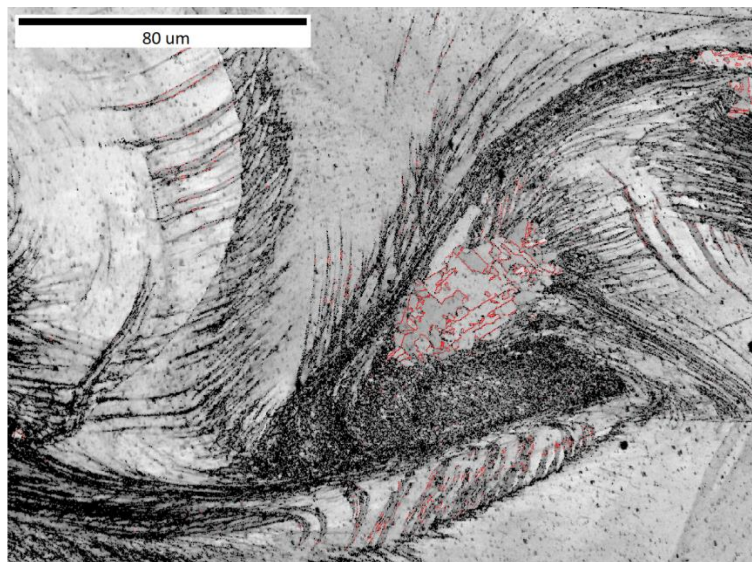

***Figure 31:** Software attempt at determining twins at 1000x.*

8. References

Andrade, U., Meyers, M. A., Vecchio, K. S., & Chokshi, A. H. (1994). DYNAMIC RECRYSTALLIZATION IN HIGH-STRAIN, HIGH-STRAIN-RATE PLASTIC-DEFORMATION OF COPPER. *Acta Metallurgica Et Materialia, 42*(9), 3183-3195. doi:10.1016/0956-7151(94)90417-0

Bacca, M., Hayhurst, D. R., & McMeeking, R. M. (2015). Continuous dynamic recrystallization during severe plastic deformation. *Mechanics of Materials, 90*, 148-156. doi:10.1016/j.mechmat.2015.05.008

Boakye-Yiadom, S., & Bassim, N. (2018). Microstructural evolution of adiabatic shear bands in pure copper during impact at high strain rates. *Materials Science and Engineering a-Structural Materials Properties Microstructure and Processing, 711*, 182-194. doi:10.1016/j.msea.2017.11.027

Fullman, R. L., & Fisher, J. C. (1951). FORMATION OF ANNEALING TWINS DURING GRAIN GROWTH. *Journal of Applied Physics, 22*(11), 1350-1355. doi:10.1063/1.1699865

Haouaoui, M., Hartwig, K. T., & Payzant, E. A. (2005). Effect of strain path on texture and annealing, microstructure development in bulk pure copper processed by simple shear. *Acta Materialia, 53*(3), 801-810. doi:10.1016/j.actamat.2004.10.032

Humphreys, F. J., & Hatherly, M. (1995). *Recrystallization and Related Annealing Phenomena*. Pergamon: Elsevier Science Ltd.

Meyers, M. A., Nesterenko, V. F., LaSalvia, J. C., Xu, Y. B., & Xue, Q. (2000). Observation and modeling of dynamic recrystallization in high-strain, high-strain rate deformation of metals. *Journal De Physique Iv, 10*(P9), 51-56. doi:10.1051/jp4:2000909

Nassiri, A., Vivek, A., Abke, T., Liu, B., Lee, T., & Daehn, G. (2017). Depiction of interfacial morphology in impact welded Ti/Cu bimetallic systems using smoothed particle hydrodynamics. *Applied Physics Letters, 110*(23), 5. doi:10.1063/1.4984742

Sun, L. G., He, X. Q., & Lu, J. (2018). Nanotwinned and hierarchical nanotwinned metals: a review of experimental, computational and theoretical efforts. *Npj Computational Materials, 4*, 18. doi:10.1038/s41524-018-0062-2

Tang, L., Chen, Z. Y., Zhan, C. K., Yang, X. Y., Liu, C. M., & Cai, H. N. (2012). Microstructural evolution in adiabatic shear bands of copper at high strain rates: Electron backscatter diffraction characterization. *Materials Characterization, 64*, 21-26. doi:10.1016/j.matchar.2011.11.011

Tanner, A. B., & McDowell, D. L. (1999). Deformation, temperature and strain rate sequence experiments on OFHC Cu. *International Journal of Plasticity, 15*(4), 375-399. doi:10.1016/s0749-6419(98)00061-8

Vivek, A., Hansen, S. R., & Daehn, G. S. (2014). High strain rate metalworking with vaporizing foil actuator: Control of flyer velocity by varying input energy and foil thickness. *Review of Scientific Instruments, 85*(7), 8. doi:10.1063/1.4884647

Vivek, A., Hansen, S. R., Liu, B. C., & Daehn, G. S. (2013). Vaporizing foil actuator: A tool for collision welding. *Journal of Materials Processing Technology, 213*(12), 2304-2311. doi:10.1016/j.jmatprotec.2013.07.006